Aalborg University

Master Thesis in Materials Technology

Experimental Study of Fatigue Crack Propagation in Silver Soldered Compact Tension Specimen

Author:
Lukus S. Quinn

Supervisors:
Jan Schjødt-Thomsen
Jens H. Andreasen

The Faculty of Engineering and Science
Department of Materials and Production

31st of January 2022

AALBORG UNIVERSITY
STUDENT REPORT

AALBORG UNIVERSITY
STUDENT REPORT

Tenth Semester
Engineering and Science
Materials Technology
Fibigerstræde 16
9220 Aalborg East

Title:

Experimental Study of Fatigue Crack Propagation in Silver Soldered Compact Tension Specimen

Project:

Master thesis

Project period:

October 2021 - January 2022

Author:

Lukus S. Quinn

Supervisors:

Jan Schjødt-Thomsen
Jens H. Andreasen

Number of pages: 25
Number of appendix pages: 12
Total number of pages: 37
Ended: 31/01-2022

Abstract:

In this report the influence of fatigue crack propagation in silver soldered compact tension specimen was investigated using fatigue testing. Experiments were performed on the specimens subjected to cyclic tension loading using a Universal Testing Machine. Furthermore, the rate of crack growth and stress intensity factor range were to be obtained from the experimental data. Determination of the Paris Law parameters was also an important aspect of this study. Lastly, microscopy was used in order to explain how the crack propagates through the specimen.

Preface

This master thesis was written by the undersigned author as part of the Master's degree in Materials Technology at the Department of Materials and Production at Aalborg University. The IEEE citation style has been employed for literature reference. Equations and figures are abbreviated as Eq. (#) and Fig. #, respectively, and the numbering is done according to their respective chapter and section.

Acknowledgements

The author wishes to thank supervisors Jan Schjødt-Thomsen and Jens H. Andreasen for guidance with both the theoretical and experimental parts of this project.
The author also wishes to thank Ole Danielsen and Henrik Nielsen for help with sample preparation, Thomas S. Quaade for preparing the etching solution, and Fahimeh Shakibapour for help with the fatigue testing machine.

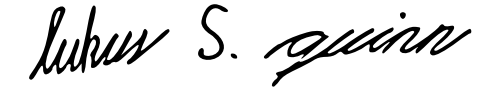

Lukus S. Quinn

Contents

Chapter 1

Introduction

Electronic devices have become central to our modern society. In most devices power modules are present and critical for the function of the device. Therefore it is of great importance that these modules are reliable[1, 2]. Power modules consists of different materials soldered together, see Fig. 1.1 for a schematic of a typical power module.

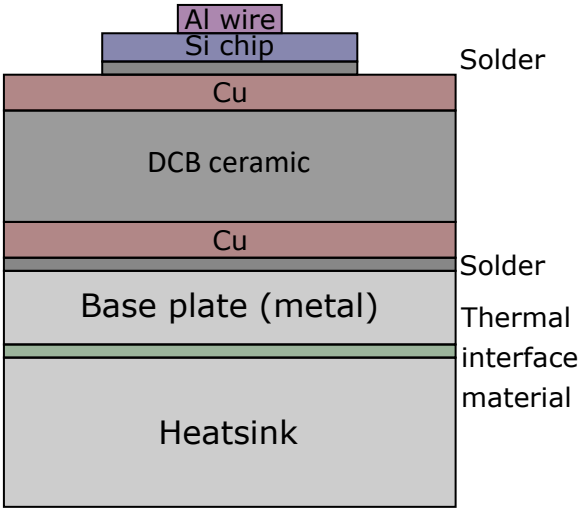

FIGURE 1.1: IGBT power module schematic.

The different materials possess different thermal coefficients, meaning that they respond differently to temperature gradients. Therefore, thermomechanical stresses arise within the power modules as they are powered on and off. These stresses can lead to multiple different types of failure mechanisms, which include bond wire fatigue, solder fatigue, and metallization reconstruction, among others. Bond wire fatigue can be caused by degradation of the wire interface and the resulting loss of contact to metallization.[3] Solder fatigue is primarily caused by temperature fluctuations. Typically solder fatigue does not lead to a substantial increase in resistance, however the loss of contact to the heatsink can lead to an increase in mean temperature which results in altered performance of the power module. Metallization reconstruction increases the resistance of the aluminium sheet, increasing temperatures and affecting performance [4].
Usually, when investigating solder fatigue in power modules either power cycling, thermal cycling, or isothermal mechanical testing is performed, where the power cycling test is the main qualification test to validate lifetime of power modules. However, studies using those test methods have been presented in numerous studies for solder

fatigue in power modules[5]. Instead, a common approach utilizing fracture mechanics to an uncommon specimen configuration has been done for the experimental part of this project. This project is focused on examining the fatigue crack propagation of solder joints, such as those present in power modules.

Chapter 2

Linear Elastic Fracture Mechanics and Fatigue

In this section, basic linear elastic fracture mechanics and fatigue theory will be presented.
This section is based on [6] and [7]. Fatigue is in general the weakening of a material due to repeated loading and unloading of the material. Fatigue cracks will eventually begin to form and will grow during each subsequent cycle. Once the fatigue crack reaches a size where the stress intensity factor exceeds the fracture toughness of the material, the crack will begin propagating rapidly, resulting in the structural failure of the material.

2.1 Fluctuating Stress

Fatigue is caused by fluctuating stress, which means is characterized by maximum stress, σ_{max}, and minimum stress, σ_{min} which is visualized in Fig. 2.1.

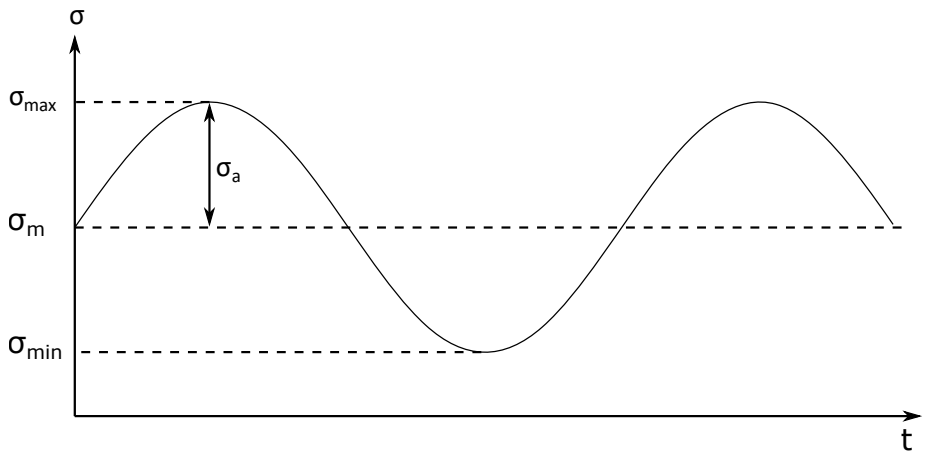

FIGURE 2.1: Constant fluctuating stress showing min, max, mean, and amplitude stress.

The amplitude and the mean stress is defined as

$$\sigma_a = \frac{\sigma_{max} - \sigma_{min}}{2} \tag{2.1}$$

$$\sigma_m = \frac{\sigma_{max} + \sigma_{min}}{2} \tag{2.2}$$

The stress ratio R is found by

$$R = \frac{\sigma_{min}}{\sigma_{max}} \tag{2.3}$$

2.2 Crack as Stress Raisers

There are different modes that define the characteristics of cracks, as seen in Fig. 2.2. In this project only cracks of mode 1 are considered.

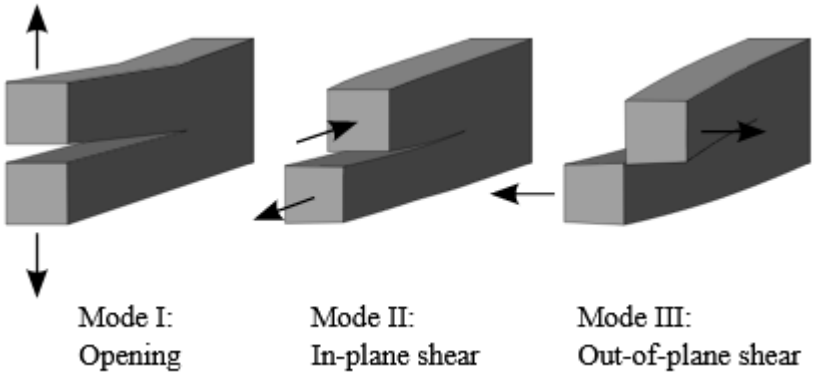

FIGURE 2.2: The three different modes of crack displacement.

Consider cracked plate, where the crack is located in center. The linear elastic stresses around the tip of the crack can be expressed using a polar coordinate system with the tip as the origin. This yields

$$\begin{aligned}
\sigma_x &= \frac{K_I}{\sqrt{2\pi r}} \cos\frac{\theta}{2}\left[1 - \sin\frac{\theta}{2}\sin\frac{3\theta}{2}\right] \\
\sigma_y &= \frac{K_I}{\sqrt{2\pi r}} \cos\frac{\theta}{2}\left[1 + \sin\frac{\theta}{2}\sin\frac{3\theta}{2}\right] \\
\tau_{xy} &= \frac{K_I}{\sqrt{2\pi r}} \cos\frac{\theta}{2}\sin\frac{\theta}{2}\sin\frac{3\theta}{2} \\
\sigma_z &= 0 (\text{plane stress}) \\
\sigma_z &= \nu(\sigma_x + \sigma_y) \quad (\text{plane strain; } \epsilon_z = 0) \\
\tau_{yz} &= \tau_{zx} = 0,
\end{aligned} \tag{2.4}$$

where K_I is called the stress intensity factor and ν is Poisson's ratio. The stress intensity factor is given by

$$K_I = \sigma\sqrt{\pi a}. \tag{2.5}$$

Here a is half the width of the crack. For the case $\theta = 0$, the expression for σ in Eq. (2.4) reduces to

$$\sigma_x = \sigma_y = \frac{K_I}{\sqrt{2\pi r}}. \tag{2.6}$$

From Eq. (2.6) it can be seen that as r approaches zero, the stress goes to infinity. In reality infinite stress is impossible, instead the material deforms around the tip of the crack, leading to the tip being blunted. The area where the material is deformed is called the plastic zone.

2.3 Fatigue Crack Growth

For average values of the stress intensity factor range, often there is a straight line on logarithmic representation of the fatigue crack growth rate, da/dN versus ΔK. Here it is shown in region II of Fig. 2.3. This line is expressed as Eq. (2.7) which is known as Paris' law [8]

$$\frac{da}{dN} = C\,(\Delta)^m\,, \tag{2.7}$$

where C is an intercept constant and m is the slope on the log-log scale.

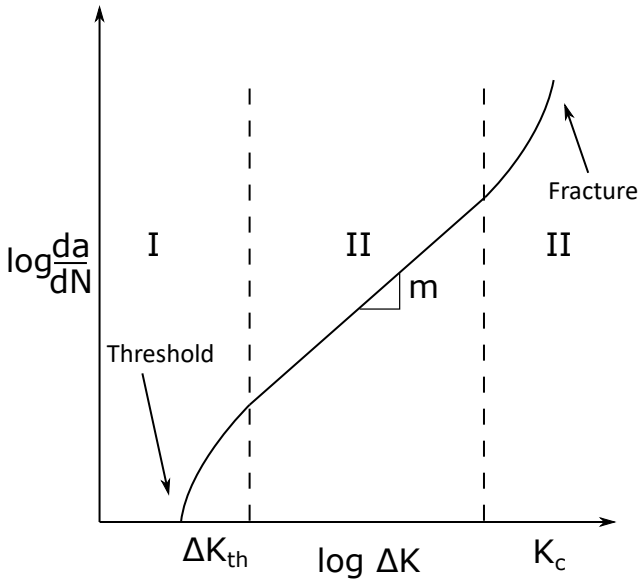

FIGURE 2.3: The three stages of crack growth for stress factor intensity range ΔK.

Tails at the upper and lower ends are typical for the growth rate curve. The tail at the lower end for small values of ΔK (region I) approaches a threshold value called the fatigue crack growth threshold, ΔKth. Crack growth does not typically occur for stress intensity ranges below the threshold.

Chapter 3

Methods

3.1 Sample Preparation

When performing fatigue crack propagation experiments, numerous specimen configurations can be chosen, such as the compact tension specimen, the middle tension specimen, the disc-shaped compact specimen, etc. The compact tension specimen, C(T), was chosen for the experiments performed under this project. This type of specimen is often used in fracture mechanics to establish fracture toughness and fatigue crack growth data. It is a single edge-notch specimen loaded in tension. The general proportions of the standard configuration is shown in 3.1. Here it can be seen that the thickness, B, and width, W, may be varied within the range $W/20 \leq B \leq W/4$. However, certain minimum dimensions are required such as the length from the center of the point of load application to the crack tip, which is known as the machined notch, a_n, must be at least 0.2W in length, W must be at least 25 mm, and the notch thickness, N, must be less than $W/16$ mm. Furthermore, the crack length, a, is measured from the crack tip to the center of the point of load application.

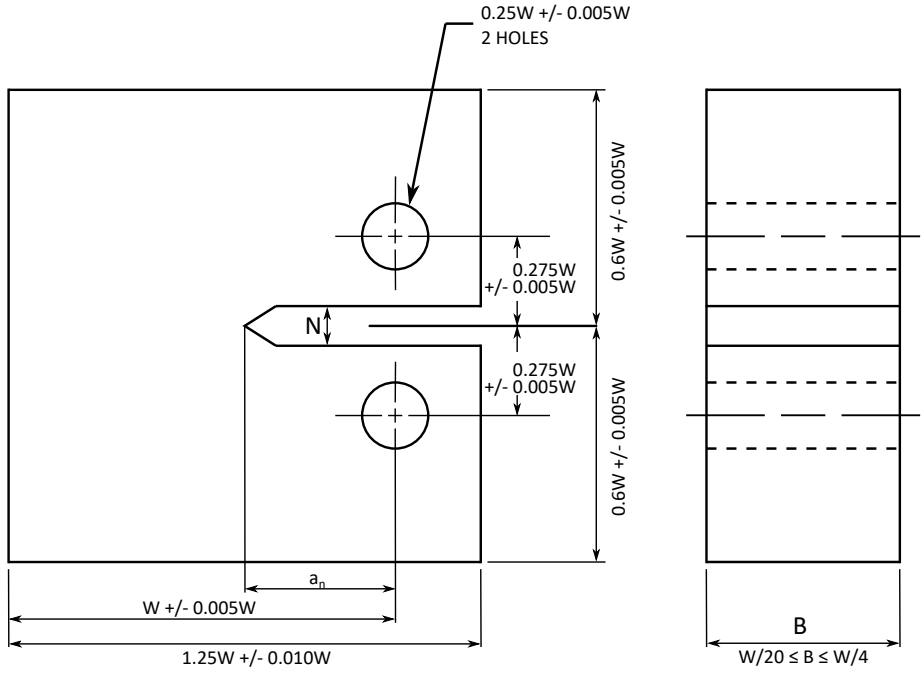

FIGURE 3.1: Standard proportions of a C(T) specimen used for determining fatigue crack growth rates.

Since determining fatigue crack growth rates is a main objective of the experimental work done during this project, standard procedures for obtaining said parameters are to be followed – the ones chosen were standards by the American Society of Testing and Materials (ASTM). The procedure, test specimen geometry, and calculations were in accordance with ASTM E399[9] and ASTM E647[10].

The geometry and dimensions chosen for the specimen used in this project can be seen in Fig. 3.3. Additionally, a machined knife edge was added at the start of the notch for positioning of a crack gauge which measures the mechanical displacement at the front of the specimen during the experiments (more about this in Section 3.2). See Fig. 3.2 for details about the dimensions of the knife edge designed according to ASTM E399.

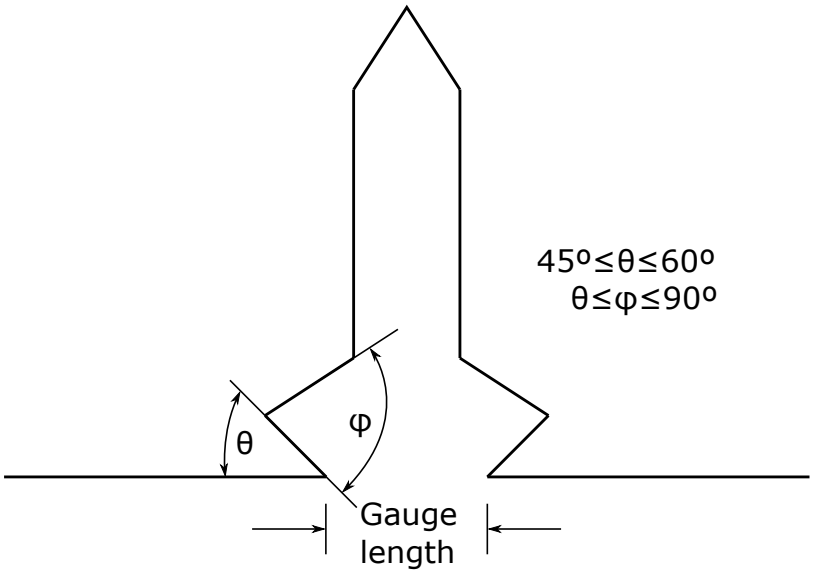

FIGURE 3.2: Geometry of the straight through notch used in this project.

The final important parameters for the C(T) specimen ended up as follows: $W = 40$ mm, $B = 5$ mm, and $a_n = 8$ mm – they are important since they are included in the equations used to calculate the stress intensity factor range. Thus, the above-mentioned requirements are fulfilled for a standard C(T) specimen.

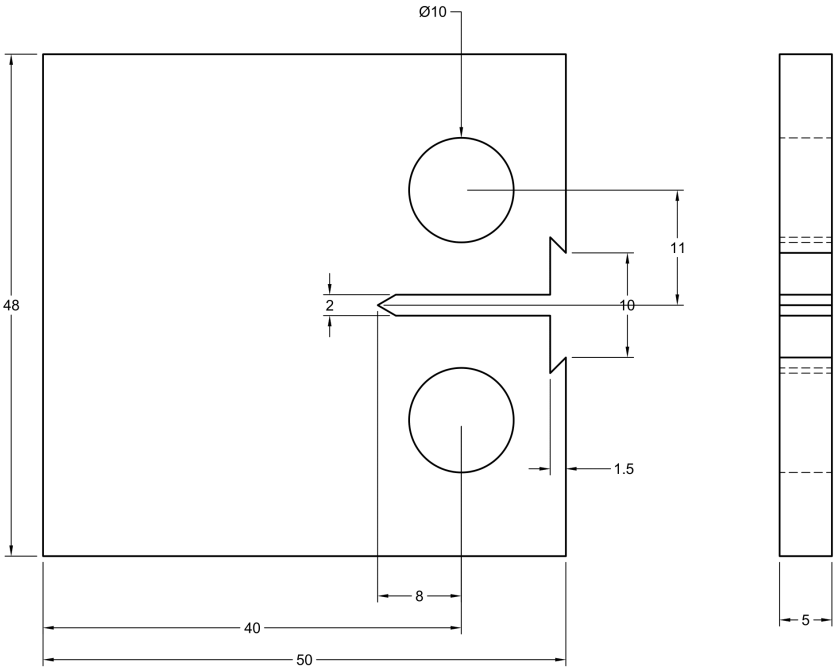

FIGURE 3.3: Dimension and geometry of the specimen and notch used in this project. All lengths are in mm.

The dimensions of the specimen were chosen based on the materials and equipment available at the institute e.g. the specimen were cut from a copper plate found at the institute, but this plate had a thickness of 5 mm so this already set certain limits on the dimensions. Choosing a width of 40 mm yields a diameter for the pin holes to be 10 mm which was also taken into account since certain sizes of clevises and pins for loading application were already available at the institute. Therefore new fixtures were not required to be made which saves time – Furthermore, the crack notch and knife edge were designed based on the gauge length of the extensometer available.

In order for results to be valid it is required that the specimen be predominantly elastic at all values of applied force. The minimum in-plane specimen sizes to meet this requirement are based primarily on empirical results. For the C(T) specimen this means that the following must be applicable:

$$(W - a) \geq (4/\pi)(K_{\max}/\sigma_{YS})^2, \tag{3.1}$$

where $(W - a)$ is equal to the specimen's uncracked ligament length, $K_{\max}$ is the maximum value of the stress intensity factor in a cycle, and σ_{YS} is the 0.2 % offset yield strength.

Orientation of the crack plane and direction of crack growth are important factors to consider as well since the fracture toughness of a material depends on such parameters in relation to the anisotropy of the material. For specimen with rectangular sections, it is common to designate a two letter code to ones specimen using a hyphenated code defined in Terminology E 1823 where the first letter represents the direction normal to the crack plane and the second letter represents the anticipated direction of crack extension. See Fig. 3.4 for different configurations of specimen aligned with the reference direction. In this project a configuration similar to L-T was used, so the specimen had the material grains oriented perpendicular to the direction of crack propagation.

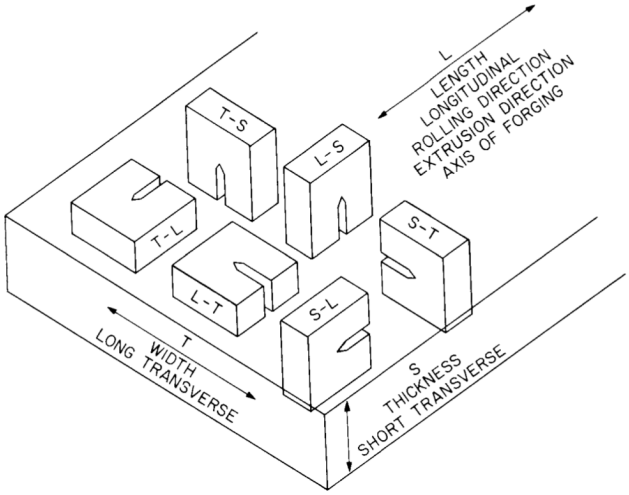

FIGURE 3.4: Specimens aligned with reference direction, and their designated two letter hyphenated code. From ASTM E399[9].

3.1.1 Manufacturing Process

The process of manufacturing the specimen can be summarized in the following steps:
- Cut a copper plate into 5x30x60 mm pieces
- Solder the pieces together
- Mill to specified dimensions and the holes into the specimen
- Edge the notch and knife edge into the specimen using electrical discharge machining (EDM)

In-between each step, the surface of each specimen was wet ground with SiC paper of increasing grit sizes from P120 to P800 grits to remove coarse scratches. Grinding the specimen is crucial since this assures a smooth surface for soldering and for the crack to initiate at the notch crack tip during the crack growth experiment – fatigue cracks show up at locations where high cyclic stresses occur such as at a discontinuity like a change in the cross section, stamp marks, improper assembly etc. Thus, if large preexisting flaws existed in the specimen it could be detrimental, and results obtained from experiments should perhaps be forsaken.
A band saw by Jakobsen (model SN 350) was used to cut the copper plate into smaller pieces. Afterwards, the copper pieces were to be soldered together – the chemical composition of the solder used for this is shown in Table 3.1. This was done by applying flux to the edges that were to be soldered, pressing them together as closely as possible, and then heating the solder to its melting temperature (630 – 660 °C) using an oxygen/acetylene torch. The liquid solder will be drawn into the gap

(a) Newly soldered specimen. The orange is copper, the white is silver solder, and the black is copper oxide formed by oxygen reacting to the heated copper metal.

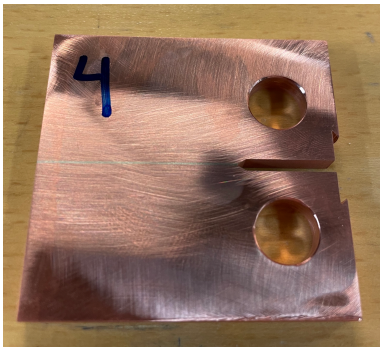

(b) Image of specimen 4 after all manufacturing steps have been completed.

by capillary action, mostly filling the gap if flux is applied sufficiently to the copper. Flux is used since it removes residual oxides from the surfaces that are to be joined, protect the surfaces from re-oxidation during heating and promote the wetting of the surfaces. See Fig. 3.5a for an image of a newly soldered specimen.
After grinding excess solder and copper oxide from the specimen they were milled to the specified above-mentioned dimensions using a 4-axes tool milling machine (model MAHO MH 800 E). Lastly, the machined notch was made by using EDM with a notch root radius of 0.25 mm.
Fig. 3.5b shows an image of specimen 4.

TABLE 3.1: Composition of the solder investigated in this project

Element	Ag	Cu	Zn	Sn
Composition [%]	55	21	22	2

Although various accurate machinery was used for the manufacturing process of the specimens, soldering and grinding were done by hand. This could perhaps explain the deviation in the location of the solder joints and notch. Fig. 3.6 shows how different samples stack on top of another. Thus, the samples are not identical, and therefore different results may appear.

FIGURE 3.6: Specimen stacked on top of one another displaying the inaccuracy in the location of the machined notch

3.2 Fatigue Testing

Fatigue testing was conducted on C(T) specimen loaded in mode 1, such that only tensile forces are considered. Since da/dN-ΔK plots are to be constructed, and Paris law parameters are obtained from the plots, the stress intensity factor, K_I, is going to be determined from the experimental data. K_I depends on the applied force and crack length. The applied force is given by the equipment for each cycle, however the crack length has to be obtained by different means. The crack length can be obtained either visually or by an equivalent method as a function of elapsed fatigue cycles. These data are then subjected to numerical analysis to establish the rate of crack growth. In this project, the crack length is determined using the Crack Mouth Opening Compliance method outlined in the ASTM E399 standard. This method utilizes a strain gauge located at the crack mouth which measures the displacement between the two teeth on the knife edge of the specimen.
The test procedure for each specimen includes the following steps:

- Position the specimen in the Universal Testing Machine (UTM) and attach the Crack-Opening Displacement Gauge (CODG) to the knife edge
- Calibrate the strain gauge and balance the load indicator
- Set allowed force and strain range
- Run the fatigue program
    a) Go to mean force in 5 s.
    b) Start cyclic loading at given amplitude and frequency
    c) Stop and unload in 5 s when limits are reached

The tests were performed at a frequency of 5 Hz. This was decided based on other what other similar studies used, and since cycling the specimen at 10 Hz or above can induce inertia in components of the testing machine. Furthermore heating of the specimen often becomes problematic at higher speeds.
Mean force and force amplitude varied between certain samples (see Section 4.1).

Results obtained from the experiments include: total cycles, elapsed cycles, minimum load, maximum load, minimum strain, maximum strain. They were collected as a .csv

file. Since the fatigue tests were assumed to last more than 10^5 cycles, a huge amount of data would be acquired if the computer was to collect data for each cycle. Instead, the software was programmed to less save data by only saving at certain cycles. Each parameter was saved for the first 10 cycles, then every 10th cycle up to 100 cycles were saved, then every 100th cycle up to 1000 cycles, and afterwards every 1000th cycle was saved.

3.2.1 Test Setup

The equipment used for conducting the fatigue tests was a 100 kN hydraulic (INSTRON Schenck Hydropuls PSB) Universal Testing Machine (UTM), see Section 3.2.1 for a specimen loaded in the UTM. The software used for controlling and setting up the UTM for fatigue testing was WaveMatrix.

FIGURE 3.7: A specimen loaded in the test setup for crack propagation experiment.

The samples were fixed to the UTM with a load clevis. Fig. 3.8 shows how the specimen were secured in the clevis. As seen, flat washers were inserted in order for the specimen to be secured so minimum movement in the transverse direction to the load application transpired.

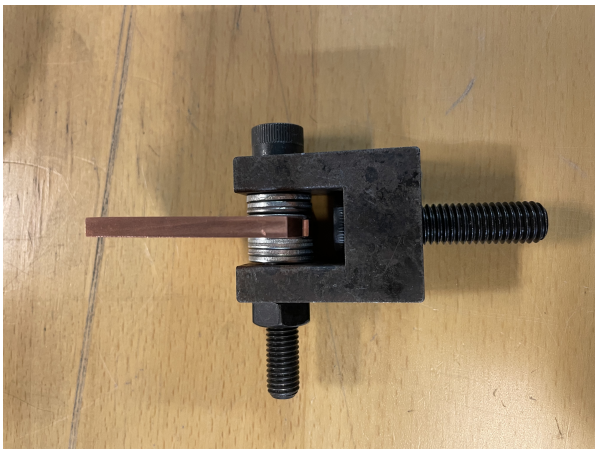

FIGURE 3.8: Sample inserted in clevis used for mounting the specimen to the UTM.

The strain gauge used for measuring the displacement at the crack mouth was an Instron C.O.D Gauge Extensometer. It is a crack mouth opening displacement (CMOD) gauge capable of measuring the distance between the teeth at the knife edge, known as the mouth opening distance.

A Point Grey camera was used for monitoring the crack propagation during the experiments. Since fatigue tests typically last many cycles the camera was set to only capture an image every 10 minutes corresponding to every 3000 cycles. The software used to capture the images was FlyCapture. Prior to conducting the experiments, a lamp was directed towards the sample for a reliable and regular light source throughout the experiment. Output settings were adjusted accordingly, and the lens was focused onto the sample.

All experiments were conducted in Aalborg University laboratories (East campus) at ambient temperatures.

Calculating Stress Intensity Factor Range and da/dN

The first step in calculating the stress intensity factor range was to calculate the crack size at every cycle using CMOC measurements. For a CT specimen, the normalized crack size is calculated as follows:

$$\frac{a}{W} = 1.000 - 4.500 \cdot U + 13.157 \cdot U^2 - 172.551 \cdot U^3 + 879.944 \cdot U^4 - 1514.671 \cdot U^5, \tag{3.2}$$

where W is the width of the specimen, and:

$$U = \frac{1}{1 + \sqrt{\frac{E' B_e V_m}{P}}} \tag{3.3}$$

for which V_m is the crack mouth opening displacement, P is the applied force, E' is the effective Young's Modulus (equal to E for plane stress as for this case), and B_e is

equal to the thickness, B, for this specimen.
The stress intensity factor range can then be calculated using the following:

$$\Delta K = \frac{\Delta P}{B\sqrt{W}} \cdot f\left(\frac{a}{W}\right), \tag{3.4}$$

where:

$$f\left(\frac{a}{W}\right) = \frac{\left(2+\frac{a}{W}\right)\left[0.886 + 4.64\frac{a}{W} - 13.32\left(\frac{a}{W}\right)^2 + 147.2\left(\frac{a}{W}\right)^3 - 5.6\left(\frac{a}{W}\right)^4\right]}{\left(1-\frac{a}{W}\right)^{3/2}}. \tag{3.5}$$

Since the computed da/dN is an average rate over the $(a_{i+1} - a_i)$ increment, the average crack size, $\bar{a} = 1/2(a_{i+1} + a_i)$, is normally used to calculate ΔK.

Calculating the crack growth rate requires use of a data reduction technique. Different techniques exist but the one chosen here is the secant method given in the ASTM 647 standard. This technique involves calculating the slope of the straight line connecting two adjacent data points on the a vs. N curve. This is also expressed as:

$$(da/dN)_{\bar{a}} = (a_{i+1} - a_i)/(N_{i+1} - N_i). \tag{3.6}$$

3.3 Vickers Hardness

The Vickers hardness [11] test is used to measure the hardness of a material. This is done by pressing a diamond pyramid tip into the material producing an indentation which area is to be determined, as shown in Fig. 3.9.

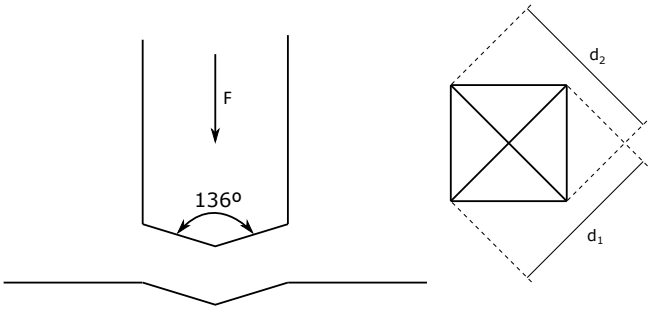

FIGURE 3.9: The left side shows the diamond tip and indentation and the right side is a visualisation of the indentation with the diagonals d_1 and d_2.

Vickers hardness, HV, is the ratio of force and area, F/A. The area of the indentation is found by

$$A = \frac{d^2}{2 \cdot \sin\left(\frac{136}{2}\right)} \tag{3.7}$$

Where d is the average value of the crossections in the indentation, $d = \frac{d_1+d_2}{2}$, shown in Fig. 3.9.
Vickers hardness is then given as

$$HV = \frac{F}{A} = F\frac{2 \cdot \sin\left(\frac{136}{2}\right)}{d^2} \tag{3.8}$$

Ten runs were performed for each material (silver solder, silver solder/copper joint, and copper) and a mean HV and standard deviation (SD) were calculated. Two different loads were applied; one of 500 gf for when measuring silver solder, and one of 300 gf for when measuring copper. These values were determined by starting with a low load, and then ramping up until a good image was shown on the screen. The indentations should be as large as possible to maximise the measurement resolution (error is magnified as indentation sizes decrease). See Fig. 3.10 for an image of the screen and software used for the experiments.

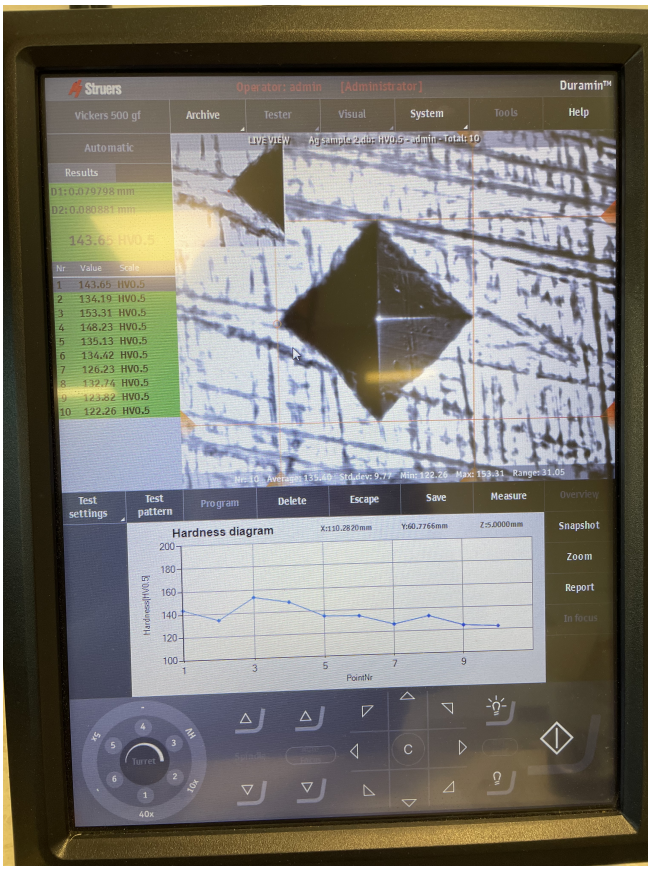

FIGURE 3.10: An image of the screen and software used for the Vickers hardness test.

3.4 Optical Microscopy

Metallographic inspection of the specimens was made in order to study the crack propagation, and also to investigate if soldering and fatigue testing influences the microstructure. Certain steps were do be done before a clear image could be established in the microscope. These steps can be summarized in the following:

- Cut the specimen into a small square capable of fitting into the polishing machine
- Cast the sample so it can be placed into the polishing machine
- The surface is polished, initially with 3 µm diamond suspension, ending with OPu until the desired smoothness is reached.
- Clean surface with acetone and apply etchant to surface for approximately 20 seconds.
- Rinse with hot water, ethanol, and then blow dry with hot air.

Chapter 4

Results and Discussion

In this chapter, the results obtained from the conducted experiments are presented and discussed.

4.1 Crack Growth Propagation

Fatigue crack growth propagation tests were conducted on six C(T) specimens. Test on the samples were conducted at different mean forces and force amplitudes, where $R = 0.1$ for all specimens. Table 4.1 shows the chosen parameters applied and the total cycles to terminated test for each specimen. The applied forces were chosen based on first an initial tensile ramp conducted, and then various force ranges were applied to a test specimen in order to decide on which forces to be applied. Although the tensile ramp did not yield any conclusive results, it did give an idea that the force should be considerably lower than the one applied. Specimen 1 was used for initial tests for deciding on what force range to be used. The mean force was increased from 800 N to 1800 N (200 N increase between each new trial), where 1800 N resulted in a large crack forming too fast. Thus 1500 N was used as the mean fore for the first experiment. As seen in Table 4.1, only a single experiment was conducted at 1500 N. The reason being that the experiment terminated at 164000 cycles. After, 1200 N was used, which resulted in favored total cycles. However, since limited specimen were manufactured, results from a lower mean force was coveted in order to investigate if mean force has an influence on the obtained Paris law parameters. Lastly, a single experiment was done using a mean force of 800 N. The reason for this is that the equipment was available for an extended time, and there was a single specimen remaining so an even lower force was applied for investigation.
Total cycles are shown to decrease with increasing mean force as suspected, the highest being 1470434 cycles for specimen 5, and the lowest being 164000 cycles. However, specimen 4 and 7 were both loaded under the same forces but the total cycles till termination were markedly different; 366319 cycles for specimen 4 and 695357 cycles for specimen 7 i.e. almost twice as many cycles for specimen 7 compared to specimen 4. Such drastic differences ought to be a result of the manufactoring process. However, no noticeable differences were observed prior to fatigue testing, and no detectable voids or damage to the solder joint was observed to have been present, see Section 4.3 for microscopic images of the specimens.

TABLE 4.1: Load values applied and total cycles to terminated experiment for each specimen.

Specimen	Mean force [N]	Force amplitude [N]	Total cycles
2	1500	1227	164000
6	1200	982	309917
3	1200	982	258314
7	1000	818	695357
4	1000	818	366319
5	800	655	1470434

After calculating the stress intensity factor range and da/dN for each specimen the da/dN vs. Δ plots were to be constructed – from here the Paris law parameters C and m could be extracted. This was done by applying a power law trend line to the data. However, before doing so many data points were removed from the whole data set. The reason being that the Paris law exclusively describes the crack propagation and not initiation or failure.
Below, da/dN vs. Δ plots are shown for each specimen, see Appendix B for photos of the propagating crack.

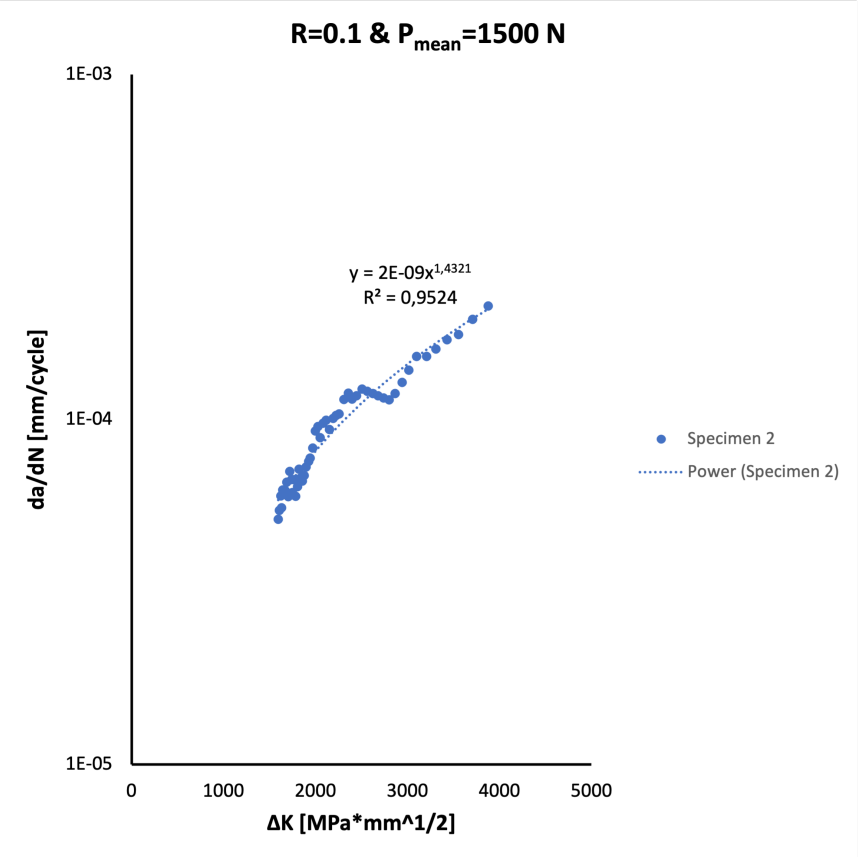

FIGURE 4.1: da/dN vs. ΔK plot of specimen 2 with a power law trend line and R^2 applied.

In Fig. 4.1, data points for da/dN vs. ΔK of specimen 2 are shown, together with a power law trend line and corresponding R^2 value. R^2 being equal to 0.9524 indicates that the data points fall along the applied power law. However, the experiment was

cut short during the test of this sample (at 30% instead of 40% strain of the strain gauge), which most likely is the reason why similar ΔK are not observed for this plot in comparison to the other plots.

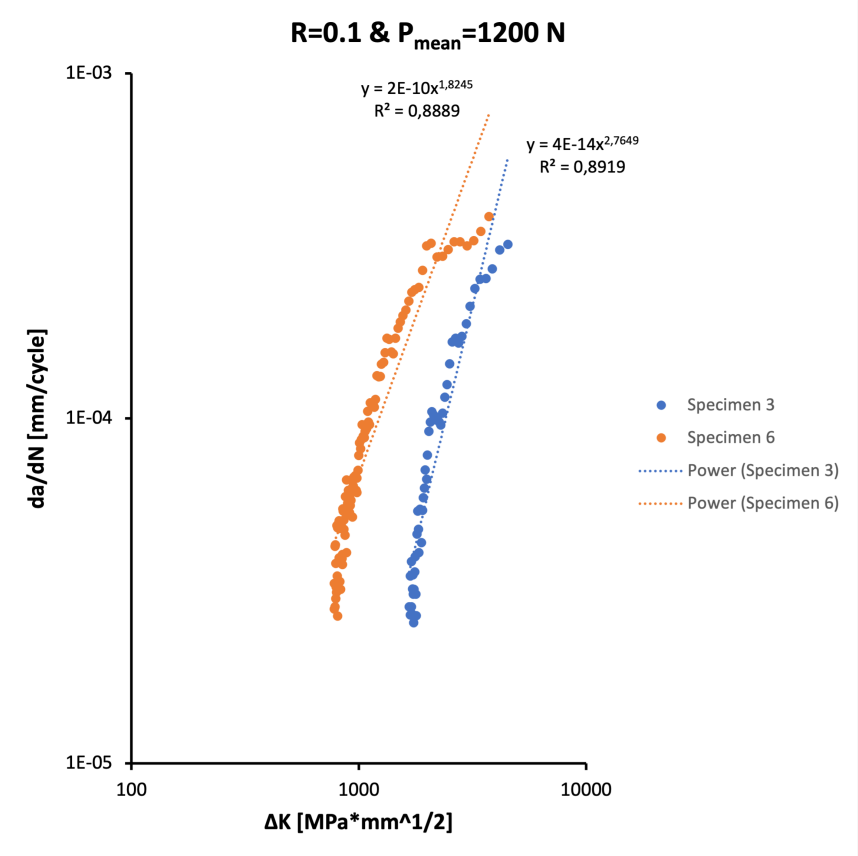

FIGURE 4.2: da/dN vs. ΔK plot of specimen 3 and 6 with a power law trend line and R^2 applied.

In Fig. 4.2, data points for da/dN vs. ΔK of specimen 3 and 6 are shown, together with a power law trend line and corresponding R^2 value. Large deviations between the two data set are shown. Several reasons for such variation are to be considered. These include how the specimens were manufactured. Although various accurate machinery was used for the manufacturing process of the specimens, soldering and grinding were done by hand. This, perhaps, resulted in deviations in the center of machined notch, as described in Section 3.1.1. Thus, resulting in an asymmetric loading situation since one side of the notch is closer to either the top or bottom loading pin.
Furthermore, the heat treatment from soldering was applied manually this most likely resulted in each specimen being heated up at altered rates and held at altered temperatures for various times, resulting in individual specimen experiencing different degrees of recrystallization, thus changing how each specimen reacts to the applied load.
Since the two specimens had different total cycles, their C and m parameters were expected to be distinct. This was also what was observed from the two data set. Specimen 3 has Paris law parameters $C = 4.45\text{e-}14$ and $m = 2.7649$ while specimen 6 has $C = 2.32\text{e-}10$ and $m = 1.8245$. Large differences are thus observed between these two samples even though an identical loading program was used for both.

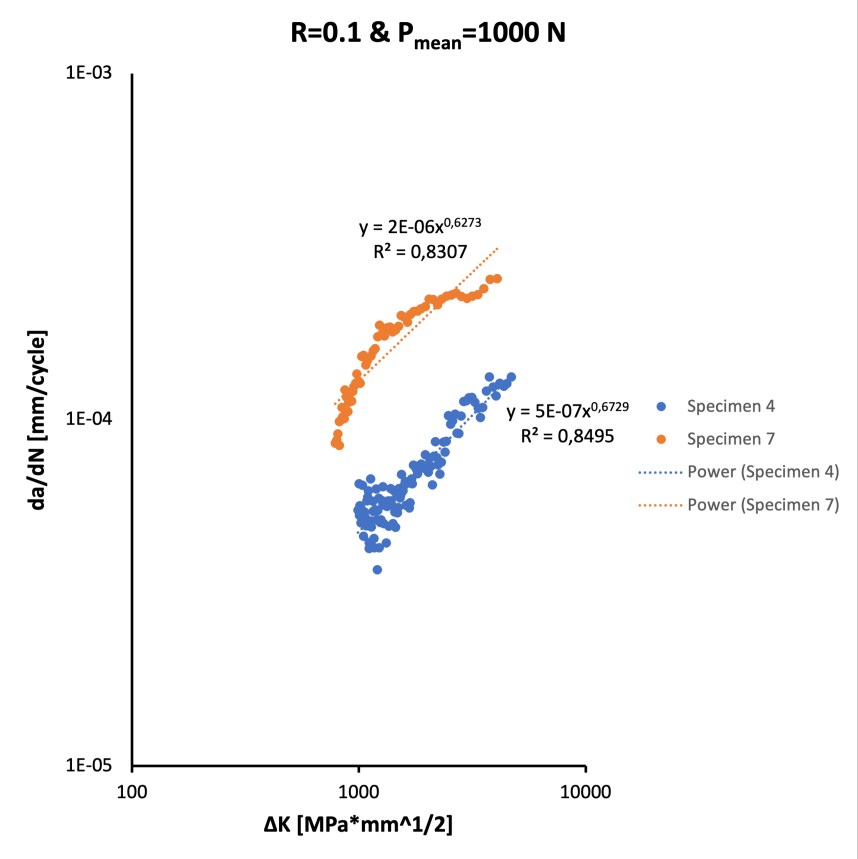

FIGURE 4.3: da/dN vs. ΔK plot of specimen 4 and 7 with a power law trend line and R^2 applied.

In Fig. 4.3, data points for da/dN vs. ΔK of specimen 4 and 7 are shown, together with a power law trend line and corresponding R^2 value. Similar discrepancies are observed between specimen 4 and 7 as for specimen 3 and 6 mentioned above, and even larger is noted between their total cycles. Specimen 4 has Paris law parameters $C = 4.55\text{e-}07$ and $m = 0.6729$ while specimen 7 has $C = 1.70\text{e-}06$ and $m = 0.6273$. Huge differences between C and m for specimen 4 and 7 are not present, even though the total cycles of specimen 7 was almost twice as much as for specimen 4. However, compared to the previous results for specimen 3 and 6, even larger differences are seen.

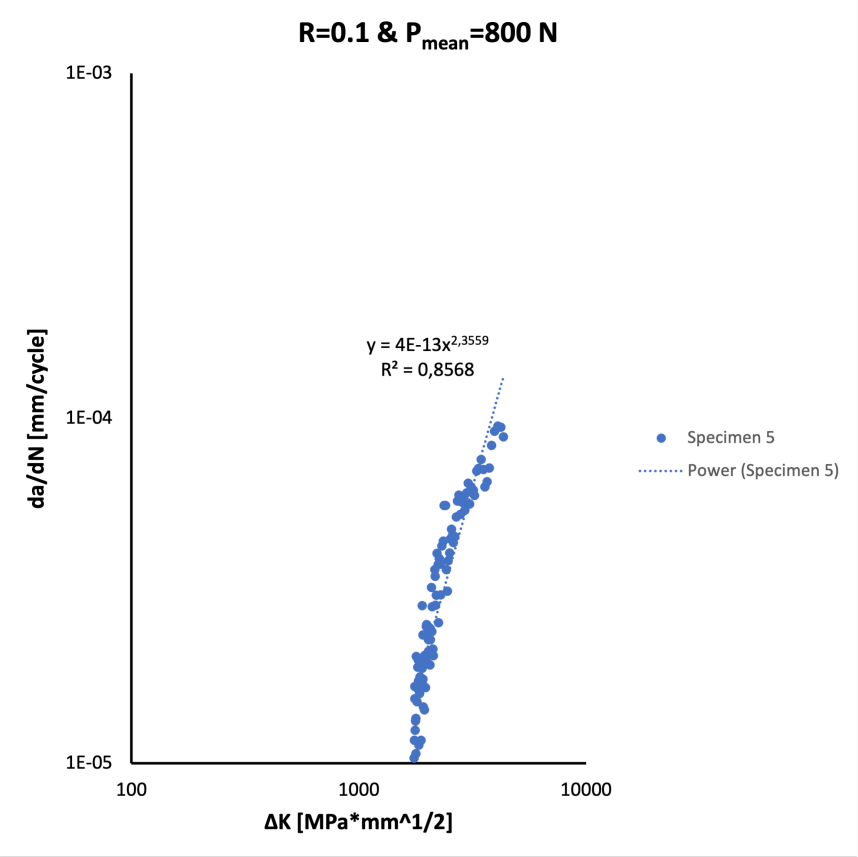

FIGURE 4.4: da/dN vs. ΔK plot of specimen 5 with a power law trend line and R^2 applied.

In Fig. 4.4, data points for da/dN vs. ΔK of specimen 5 are shown, together with a power law trend line and corresponding R^2 value.
This plot shows the lowest values yet seen for the crack growth rate, as expected for the lowest applied force, and equivalently the longest run. However, no significant values for C or m are obtained for this specimen. When comparing to the other specimen's parameters, the results from this specimen lie in-between the rest.

Since copper is a highly ductile material[12], plasticity was anticipated to occur. This did turn out to be the case, see Appendix B which shows plasticity being present after the experiments have been conducted.

Residual stresses are also factors which should be considered since if present may influence the fatigue life and also the crack growth during fatigue testing. However, such stresses were not investigated during this study, and can thus not be quantized.

It should be noted that although the C parameters given in Table 4.2 are shown with more decimals than for the da/dN vs. ΔK plots above, the C parameter is still extracted from the same plots.

TABLE 4.2: Paris law parameters, C and m, and R^2 for each specimen.

Specimen	C	m	R^2
2	1.52e-09	1.4321	0.9524
6	2.32e-10	1.8245	0.8889
3	4.45e-14	2.7649	0.8919
7	1.70e-06	0.6273	0.8307
4	4.55e-07	0.6729	0.8495
5	3.60e-13	2.3559	0.8568

Rahman Seifi et. al. [13] studied fatigue crack growth in raw and annealed pure copper with considering cyclic plastic effects. They reported values of C between 3.76e-16 and 2.11e-14, and values of m between 3.65 and 4.17, which are values faraway from the ones obtained during this study. No trend can be made with regards to an increase or decrease to the values of C and m shown in Table 4.1. The R^2 values lie between 0.8307 and 0.9524; hence are considerably accurate.

4.2 Vickers Hardness

In Table 4.3, HV values of the materials obtained from the Vickers hardness test are presented. Each test was performed on a soldered specimen, except on the pure copper. Silver solder refers to hardness test being conducted in the middle of the solder joint, and silver solder/copper joint refers to test being conducted at the interface between the silver solder and the copper. Tests were also conducted on pure copper and on the copper of the soldered sample halfway between the specimen edge and solder joint, in order to minimise the effect of soldering on hardness. The comparison between the two copper was done in order to investigate if the heating process from soldering affected the hardness a distance away from the solder joint.

Material	Mean HV (SD)
Silver solder	139.2 (5.4)
Copper (halfway between edge and solder joint)	83.3 (4.9)
Silver solder/copper joint	116.2 (9.2)
Copper (pure)	116.3 (8.7)

TABLE 4.3: HV values of the materials investigated in this project.

As seen in the table, silver solder is the hardest material with an HV value of 139.2 with a standard deviation of 5.4. The silver solder/copper joint and pure copper have similar HV values, being 116.2 (9.2) and 116.3 (8.7), respectively. The softest of the measured materials is the copper measured on the soldered specimen. Thus, the hardness is observed to decrease under two circumstances: 1) at the interface, and 2) at the heated/annealed specimen. Annealing is known to reduce hardness of metals. This is also the case for copper shown here and documented in various other articles such as [12] by Farshad Nazari et. al.
The soldering process has thus overall reduced the hardness of the used materials.

4.3 Optical Microscopy

The surface of the specimens were investigated using optical microscopy. Different locations were observed on the specimen in order to examine if heating the specimen from the soldering process influenced the microstructure, as well as to investigate the cracks that occurred from the fatigue tests.

Below, images from the optical microscopy are shown.

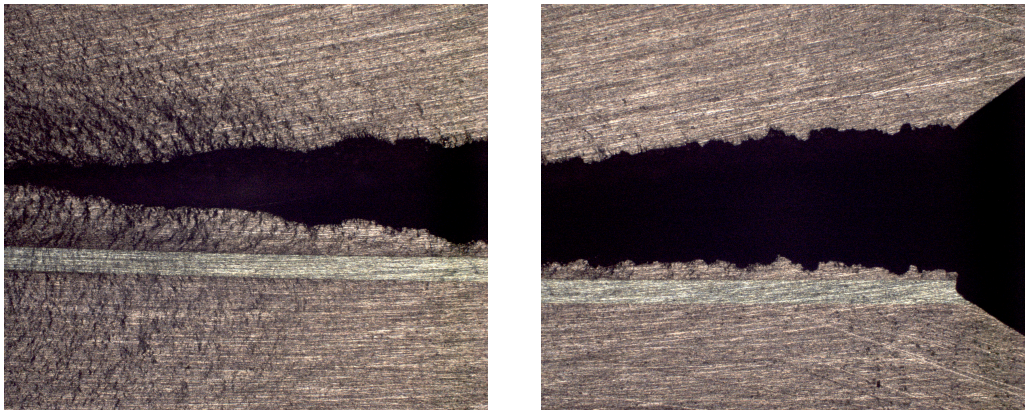

(a) (b)

FIGURE 4.5: The crack propagation in specimen 4.

As seen in Fig. 4.5, the crack has an affinity to propagate through the copper close to the copper/solder joint interface. This is the case for that specimen, as well as for all other specimens that were fatigue tested.
Even as in Fig. 4.6 where a void is clearly present in the silver solder close to the notch crack tip, the crack tends to propagate across either the silver solder/copper joint or slightly above in the copper. This figure shows a before and after image of the notch crack tip of specimen 7.

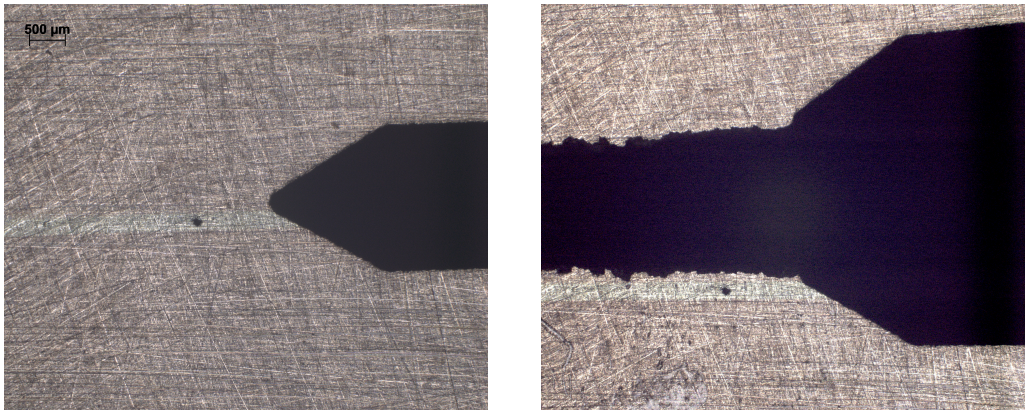

(a) (b)

FIGURE 4.6: Before and after fatigue testing on specimen 7.

Fig. 4.7 shows two images; left is an image of specimen 7 showing all the voids present on the back side of the silver solder, and right is an image of the microstructure of the silver solder and copper of a specimen. Still with these voids present, the crack did not navigate towards such an impurity. The image of the microstructure

shows the microstructure of both the copper and the silver solder. For the copper, recrystallization is clearly shown to have taken place, indicating that the heating during the thermal process has annealed the copper to a certain extent. This is also in agreement with the observed hardness results, where the hardness has been reduced in the copper compared to the pure copper.

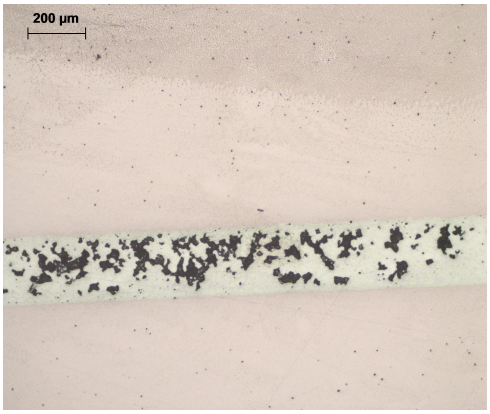

(a) Many voids observed on back side of specimen 5 (post fatigue testing).

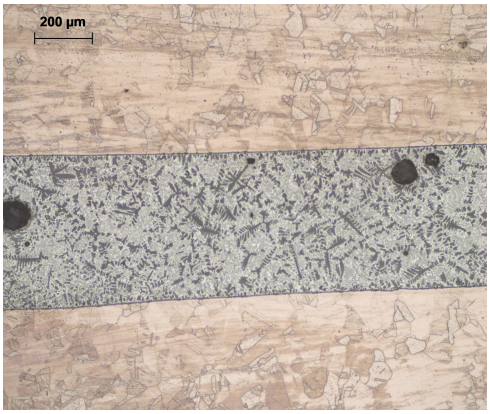

(b) Microstructure of the silver solder and copper of a specimen.

FIGURE 4.7

Although these results indicate that the crack will propagate across the joint or in the copper, never the silver solder, care should be taken if using this as a fact. As mentioned a few times throughout this report, various problems resulted in dissimilar specimen with its crack notch center misaligned with the middle of the specimen (so an asymmetrical load with be applied to the C(T) specimen during fatigue testing). However, if this phenomena is prevalent again during more accurate experiments, then this result could yield as a tremendously positive result, since this could simplify life time estimation or similar models by assuming the crack will not propagate into the silver solder.

Chapter 5

Conclusion

An experimental study was carried out on the fatigue crack growth in C(T) specimens made by silver soldering copper plates together in order to evaluate how a crack propagates though the silver solder, as well as to obtain Paris law parameters from the experimental data. Results from the fatigue tests yielded da/dN vs. ΔK plots which gave a fairly large range of different Paris law parameters. The range of C was between 4.45e-14 and 1.70e-06, and values of m between 0.6273 and 2.7649. A single set of Paris law parameters is not enough to describe crack propagation, and since specimen 2 and 5 were fatigued with their own mean force and amplitude nothing conclusive can be said from the obtained results regarding them. Plasticity is not entirely known in the crack growth propagation experiments. However, due to the specimens consisting mainly of copper, this should have been taken into consideration since copper is very ductile. By doing so perhaps a better way of figuring out which data points were induced by plasticity could have been performed. A common approach to use on materials that display elastic plastic deformation is to use the crack growth propagation through J integral approach. Manufacturing complications yielded dissimilar specimens in accordance with one another and the ASTM standard configuration, potentially discounting the results obtained. Based on the obtained results, no conclusive statements can be made about the fatigue crack growth or propagation. However, microscopic inspection of the fatigued specimens were carried out, showing that all cracks had an affinity towards propagating at the silver solder/copper interface or in the copper.

Bibliography

[1]B. K. Bose, "Global energy scenario and impact of power electronics in 21st century", IEEE Transactions on Industrial Electronics **60**, 2638–2651 (2012).

[2]L. Yang, P. A. Agyakwa, and C. M. Johnson, "Physics-of-failure lifetime prediction models for wire bond interconnects in power electronic modules", IEEE Transactions on Device and Materials Reliability **13**, 9–17 (2012).

[3]M. Ciappa, "Selected failure mechanisms of modern power modules", Microelectronics reliability **42**, 653–667 (2002).

[4]K. B. Pedersen and et. al., "Degregation in high power IBGT modules subjected to sinusoidal current load", (2015).

[5]M. Brincker, "Reliability of metal films and interfaces in power electronic devices", (2018).

[6]A. F. Bauer, *Applied Mechanics of Solids* (Taylor and Francic Group, 2010).

[7]R. L. Norton, *Machine Design, An Integrated Approach*, English, 4th (2011).

[8]P. Paris and F. Erdogan, "A critical analysis of crack propagation laws", (1963).

[9]ASTM Standard E399, "Standard test method for linear-elastic plane-strain fracture toughness k_{IC} of metallic materials", ASTM International, West Conshohocken, PA (2009).

[10]ASTM Standard E647, "Standard test method for measurement of fatigue crack growth rates", ASTM International, West Conshohocken, PA (2000).

[11]C. V. et.al, *Matallurgi for Ingeniører* (Forfatterne og Akademisk Forlag, 1998).

[12]N. Farshad, H. Mohammad, and H. Zhao, "Effect of stress relief annealing on microstructure, mechanical properties, and residual stress of a copper sheet in the constrained groove pressing process", The International Journal of Advanced Manufacturing Technology **102**, 4361–4370 (2019).

[13]R. Seifi and R. Hosseini, "Experimental study of fatigue crack growth in raw and annealed pure copper with considering cyclic plastic effects", Theoretical and Applied Fracture Mechanics **94**, 1–9 (2018).

Appendix A

Machinery used for Manufacturing the Specimens

Figure A.1

FIGURE A.2

FIGURE A.3

Appendix B

Crack Propagation Images

Below a series of images are presented which are captured using camera and setup as explained in Section 3.2.1.

B.1 Specimen 2

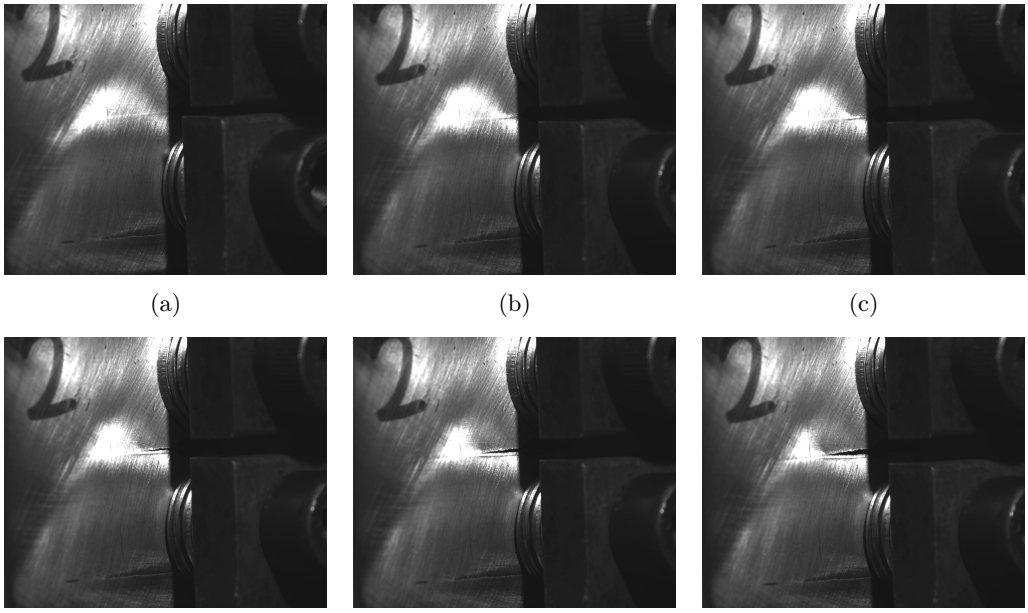

(a) (b) (c)

(d) (e) (f)

FIGURE B.1: The crack propagation of specimen 2

B.2 Specimen 3

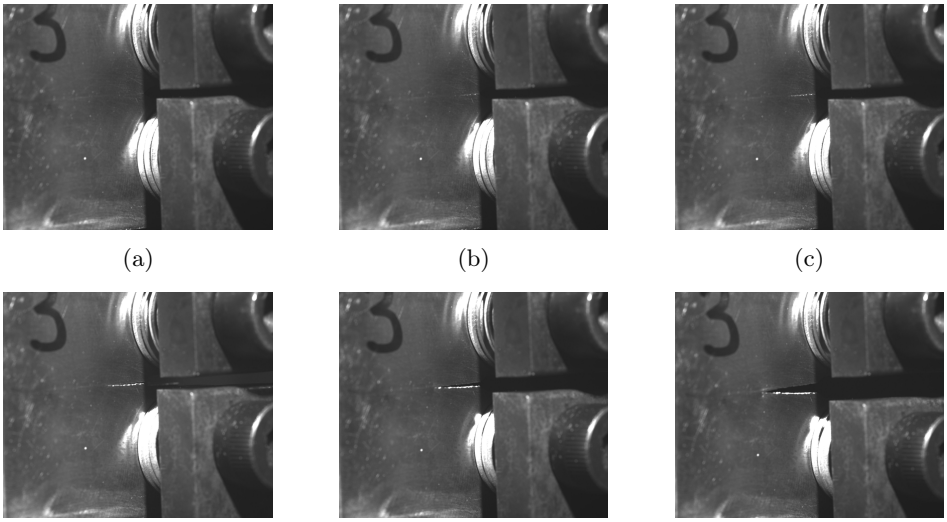

(a) (b) (c)

(d) (e) (f)

FIGURE B.2: The crack propagation of specimen 3

B.3 Specimen 4

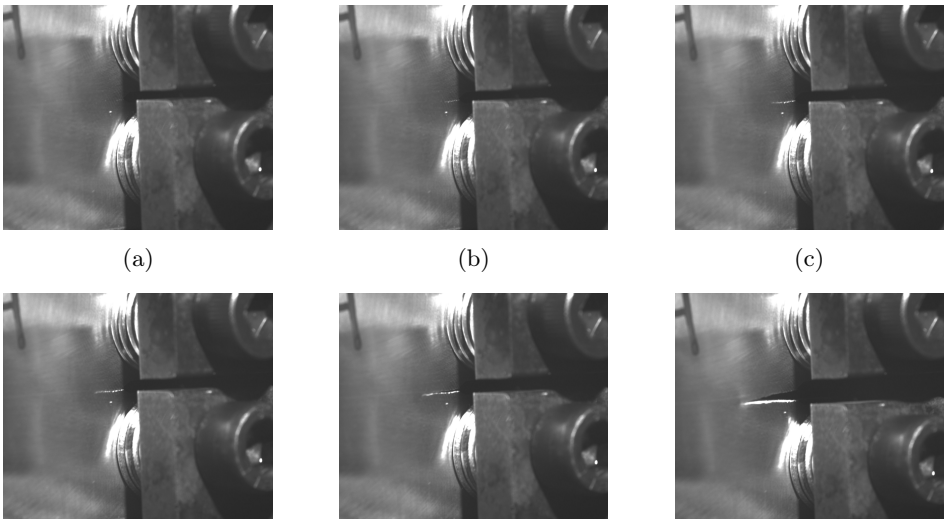

(a) (b) (c)

(d) (e) (f)

FIGURE B.3: The crack propagation of specimen 4

B.4 Specimen 5

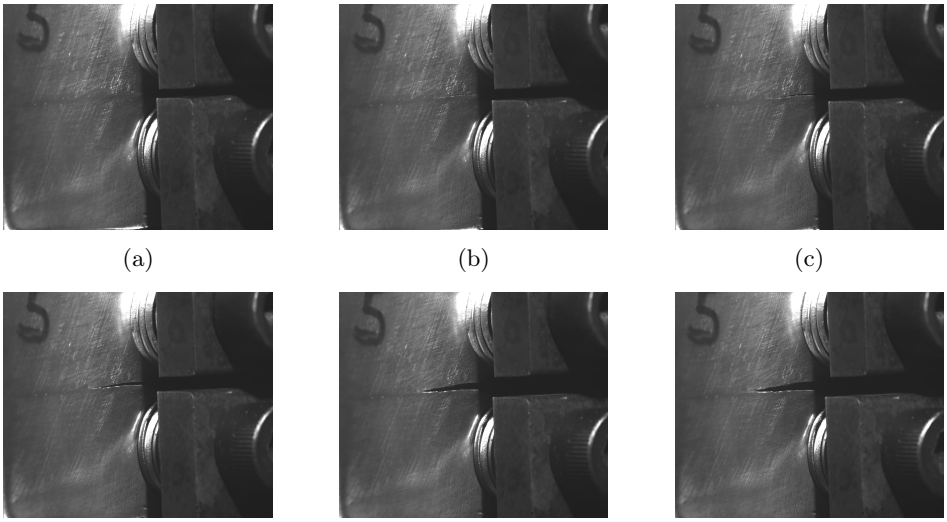

(a) (b) (c)

(d) (e) (f)

FIGURE B.4: The crack propagation of specimen 5

B.5 Specimen 6

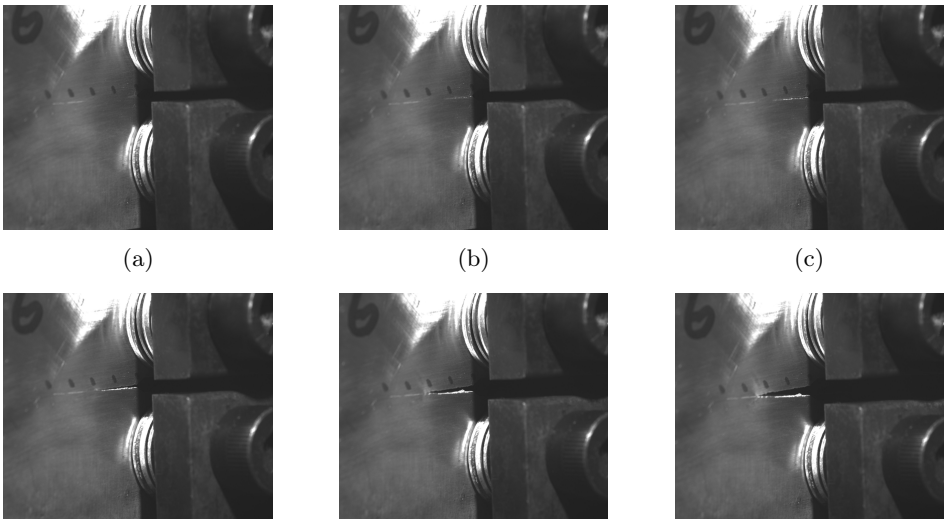

(a) (b) (c)

(d) (e) (f)

FIGURE B.5: The crack propagation of specimen 6

B.6 Specimen 7

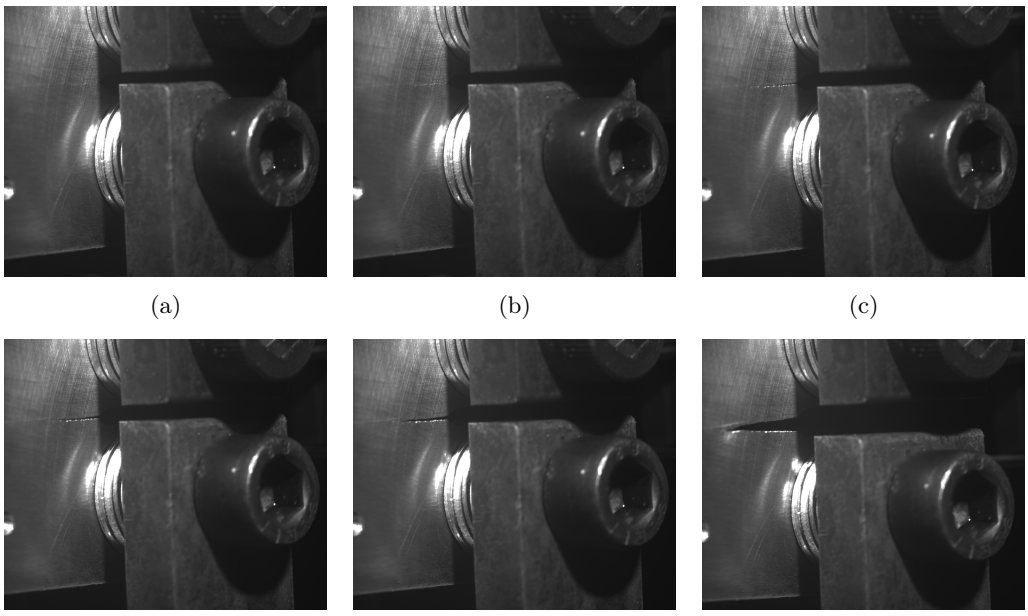

(a) (b) (c)

(d) (e) (f)

FIGURE B.6: The crack propagation of specimen 7